A Selenocysteine Variant of the Human Copper Chaperone for Superoxide Dismutase. A Se-XAS Probe of Cluster Composition at the Domain 3−Domain 3 Dimer Interface[†]

Amanda N. Barry and Ninian J. Blackburn*

Department of Environmental and Biomolecular Systems, OGI School of Science and Engineering, Oregon Health and Sciences University, Beaverton, Oregon 97006–8921

Received January 18, 2008; Revised Manuscript Received February 20, 2008

ABSTRACT: We report the semisynthesis of a selenocysteine (Sec) derivative of the human copper chaperone for superoxide dismutase, substituted with Sec at the C-terminal C246 residue. Measurements of hCCS-induced SOD1 activation were used to show that the C-terminal CXC sequence is both necessary and sufficient for EZn-SOD maturation. Therefore, an active CAU variant carrying Sec as the terminal amino acid was prepared by expressed protein ligation of a single selenocysteine amino acid to a 243-CA truncation. This reaction proceeded in high yield and generated the desired 243-CAX (X = C or U) protein with the expected mass. Se-edge XAS of the apoprotein indicated that both Se−S and Se−Se interactions were present in a 0.3:0.7 ratio, indicating an equilibrium between species with either a selenosulfide or a diselenide cross-link. After reduction on immobilized TCEP, the ligated Cys and Sec apoproteins bound up to 2.5 Cu(I) ions per hCCS monomer with both Cu and Se as constituent atoms of the cluster which forms at the domain 3 interface of a hCCS dimer. Merging of XAS data at the Cu and Se K-absorption edges provided additional details of the cluster composition, specifically the fact that both Se atoms occupied bridging positions between two Cu(I) atoms. Further, the requirement for identical Cu−Se bond lengths and Debye–Waller factors at each absorption edge allowed us to rule out simple models for the cluster composition such as a bis-Cys(Sec)-bridged dinuclear cluster and was indicative of a more complex cluster with a nuclearity of ≥3.

The human copper chaperone for Cu,Zn-superoxide dismutase (hCCS),[1] the largest of the identified copper metallochaperones, is a 27 kDa three-domain protein which functions in the maturation of its target, Cu,Zn-superoxide dismutase (SOD1) (*1–4*). Biochemical (*5, 6*) and crystallographic (*7–10*) studies have provided important details about the structural and functional properties of the individual domains of hCCS as shown in Figure 1. Like other copper metallochaperones, CCS domain 1 (D1, residues 1–85) contains the Cu(I)-binding MXCXXC motif. The function of this domain is unclear, and while studies in yeast suggest that it is only functionally important under limiting copper conditions (*6*), it appears to be essential in mammalian species (*11*). Domain 2 (D2, residues 86–234) of CCS is similar to SOD1, containing six of the seven amino acids necessary for binding of Cu and Zn. Due to substitution of a His residue with Asp, D2 is not able to bind Cu, but a gain of SOD1 activity is observed when the Asp is mutated to a His (*12*). Crystal structures of yeast CCS (yCCS) and human (hCCS) proteins reveal that the apoprotein dimerizes along a SOD-like D2−D2 dimer interface (*7, 9, 10*) and that this interface is also involved in recognition and binding of the SOD1 partner (*5, 8*). Domain 3 (D3, residues 235–274) contains a CXC Cu(I)-binding motif which is absolutely required for the metal transfer activity of the protein (*5, 6, 13, 14*). The D3 polypeptide is disordered in the yCCS structure but becomes visible in the yeast heterodimeric complex formed between yCCS and the H48F variant of ySOD1 (*8*).

The original mechanism introduced by Rae et al. (*15*) suggested that the transfer process occurs via formation of a heterodimer of CCS and SOD1. It was suggested that a copper complex formed at the CXC D3 site became intercalated into the empty SOD1 catalytic (Cu) site and that transfer proceeded via ligand exchange. A crystal structure of SOD1 H48F in complex with yCCS revealed that SOD1 interacted with the CCS metallochaperone to form a complex comprising one monomer of each protein (*8*). The functionally essential D3 C-terminus of yCCS was shown to be well-positioned to play a key role in the metal ion transfer mechanism and surprisingly was linked to SOD1 by an intermolecular disulfide bond. Further investigations suggested that SOD1 activation by CCS was a redox process

[†] The work was supported by a program project grant (P01 GM067166) from the National Institutes of Health to N.J.B.

* To whom correspondence should be addressed: Department of Environmental and Biomolecular Systems, OGI School of Science and Engineering at OHSU, 20000 NW Walker Rd., Beaverton, OR 97006-8921. Phone: (503) 748-1384. Fax: (503) 748-1464. E-mail: ninian@comcast.net.

[1] Abbreviations: CCS, copper chaperone for superoxide dismutase; D1, domain 1; D2, domain 2; D3, domain 3; DW, Debye−Waller factor; EXAFS, extended X-ray absorption fine structure; EPL, expressed protein ligation; FT, Fourier transform; hCCS, human CCS; ICP-OES, inductively coupled plasma optical emission spectrometry; MESNA, 2-mercaptoethanesulfonate; Sec, selenocysteine; SOD, superoxide dismutase; TCEP, tricarboxyethylphosphine; WT, wild type; XAS, X-ray absorption spectroscopy; yCCS, yeast CCS.

10.1021/bi8001049 CCC: $40.75
Published on Web 04/05/2008

FIGURE 1: Domain structure of CCS. Ribbon diagram of the crystal structure of yCCS (taken from Protein Data Bank entry 1JK9 for the yCCS−SOD heterodimer showing domain 3 as ordered). Domain 1 (D1) is colored pink, domain 2 (D2) blue, and domain 3 (D3) green. The sequence of hCCS up to residue 252 corresponding to the three domains is shown above, color-coded as follows: D1 in pink, D2 in blue, and D3 in green. The metal binding cysteine motifs are underlined.

dependent on the presence of O_2 and that in vivo, CCS converted the reduced E,Zn^{SH} form to the mature Cu,Zn^{S-S} active enzyme (*16, 17*). Thus, SOD1 maturation occurred by a disulfide isomerase activity of CCS, most likely proceeding via the intermediacy of the mixed CCS−SOD1 disulfide between SOD1 C57 and yCCS C229 which is observed in the CCS−SOD1 H48F heterodimer crystal structure. However, the absence of bound copper in any of the crystal structures on which this mechanistic model was built prevented the role of copper in the process from being further delineated.

In a number of studies from our laboratory, we have used X-ray absorption spectroscopy (XAS) to probe the binding of copper to hCCS and to investigate the relationship between Cu coordination and metal transfer activity. Copper binding and XAS studies have been carried out on WT hCCS (*18*) and Cys to Ser single and double mutants of the D1 CXXC and D3 CXC motifs in a maltose binding protein fusion (*13*). Analogous experiments have also been pursued in an untagged hCCS isolated using an intein self-cleaving vector (*14*), this time using Cys to Ala mutations. These studies identified the coordination chemistry at each of the D1 and D3 Cu(I) binding sites, specifically that Cu(I) forms a monomeric three-coordinate CuS_2X (X = exogenous thiol or solvent) complex at the MTCQSC site in D1 but forms a multinuclear cluster at the interface of two D3 polypeptides. Analysis of the intensity of the Cu−Cu cluster interaction in the Cys to Ala variants suggested that the nuclearity of the cluster was greater than 2 and was most consistent with a Cu_4S_6 adamantane-type species. The XAS data in conjunction with studies of oligomerization equilibrium as a function of copper loading led to an alternative model for hCCS function in which Cu(I) binding converts the apo dimer with a D2−D2 interface to a new dimer connected by cluster formation at two D3 CSC motifs. The predominance of dimer over tetramer in the cluster-containing species strongly suggested that the D2 dimer interface remains open and available for sequestering a SOD1 monomer. The work implicated the copper cluster in the reactive form but fell short of providing any mechanistic detail about the reactivity of the cluster in the redox-driven copper/thiol−disulfide exchange between hCCS and its SOD1 partner.

If SOD activation is correlated with cluster formation, then it follows that the chemistry of the activation process is likely to depend critically on the cluster composition and geometry. To date, Cu K XAS is the only spectroscopic technique to reveal the existence of the Cu(I) cluster, yet even here, the details of cluster nuclearity and structure remain sketchy. Ligand-directed XAS probes (such as Se) can provide important additional information about metal coordination (*19, 20*). In previous work, we reported a Sec-substituted azurin derivative, where Se EXAFS was used in conjunction with the Cu EXAFS to provide important new information about the cupredoxin site (*21*). In this work, we extend this approach and report the semisynthesis of hCCS substituted with selenocysteine to produce a CXU motif in D3. The protein binds Cu(I) to produce the first example of a multinuclear Cu(I) cluster containing a Cu−Se bond in a protein. We further demonstrate the utility of the ligand-directed approach via merging Cu and Se EXAFS data to produce additional structural detail on the cluster. Additionally. the Se-substituted CCS variant will provide a powerful new tool for studying metal transfer from hCCS to its partner SOD, via Se-XAS observation of the loss of copper from the Se environment of CCS.

EXPERIMENTAL PROCEDURES

Cloning, Expression, and Purification of hCCS Mutants and hSOD1. Full-length-sequence-containing plasmids were produced as follows. hCCS cDNA was PCR-amplified from a human fetal brain cDNA library by use of primers at the 5′ and 3′ termini (5′-GGCCTACCGCGGTATGGCGAC-GAAGG-3′ and 5′-CCAAGGGAATGTTCCATGGGCGATC-3′). The cDNA was cloned into the pTXB-3 expression vector (New England Biolabs) by use of restriction sites NcoI and SapI introduced into the 5′ and 3′ primers, respectively. Truncated hCCS was PCR-amplified from this construct by use of primers at the 5′ and 3′ termini [5′-ACCATGGCT-TCGGATTCGGG-3′ and 5′-AGATGGTGGCTCTTCCG-CAAGCGCAGATCTG-3′(CCS-245),5′-CCAGATGGCTCT-TCCGCAGCAAGCGCAGATCT-3′ (CCS-246), 5′-TCC-TCCCAGGCTCTTCGGCAATCGCAAGCGCA-3′ (CCS-247), or 5′-GATGGGCCGGGCTCTTCCGCACCAGATG-GTGA-3′ (CCS-252)]. The cDNA was cloned into the pTXB-3 plasmid (New England Biolabs) by use of restriction sites NcoI and SapI introduced into the 5′ and 3′ primers, respectively. Truncated C22A/C25A hCCS was PCR-ampli-

fied by use of primers at the 5′ and 3′ termini [5′-ACCATGGCTTCGGATTCGGG-3′ and 5′-AGATGGTGGCTCTTCCGCAAGCGCAGATCTG-3′ (CCS245) or 5′-CCAGATGGCTCTTCCGCAGCAAGCGCAGATCT-3′(CCS246)]. The cDNA was cloned into the pTXB-3 plasmid (New England Biolabs) by use of restriction sites NcoI and SapI introduced into the 5′ and 3′ primers, respectively. All expression constructs were confirmed by automated DNA sequence analysis.

The fusion protein contained a C-terminal intein and chitin-binding domain tag for purification on a chitin resin. This tag is cleaved upon purification. The expression was designed to start at the ATG start codon in CCS and stop at the TGA stop codon after the C-terminus of the chitin binding domain. The full expression before purification is 523 or 524 amino acids for CCS245 or CCS246, respectively.

The fusion proteins were expressed in *Escherichia coli* strain ER2566 (Novagen) after induction with isopropyl thio-β-D-galactoside (IPTG) in the presence of 500 μM $ZnSO_4$. The cells were lysed with a French pressure cell press (SLM-Aminco). The fusion proteins were purified from the soluble portion on a chitin column. The chitin beads (New England Biolabs) were packed into a column and washed with 10 volumes of 50 mM sodium phosphate buffer and 500 mM sodium chloride (pH 7.2) (column buffer). The soluble portion was diluted three times with column buffer and run over the chitin column. The column was washed with an additional 10 volumes of column buffer followed by 3 volumes of column buffer with 50 mM 2-mercaptoethanesulfonate (MESNA) (cleavage buffer). One volume of cleavage buffer was then added to the column and allowed to sit overnight. The cleavage buffer was removed from the column as the first fraction followed by three separate 1 column volume elutions. All of the fractions were saved, checked for the presence of hCCS, and, where appropriate, combined. The protein was concentrated with an Amicon Centricon ultrafiltration cell.

Recombinant human SOD (hSOD1) was cloned as a NdeI−SapI fragment generated by PCR amplification of a cDNA clone obtained from Genome Systems (GenBank accession number AA702004). PCR primers that contained restriction sites NdeI (5′) and SapI (3′) were used to amplify SOD1 cDNA. This fragment was cloned into the intein pTXB-1 vector from New England Biolabs. Recombinant human SOD was expressed in *E. coli* strain ER2566 (Novagen) after induction with IPTG in the presence of 500 μM $ZnSO_4$. The cells were lysed with a French pressure cell press. Recombinant hSOD1 was purified from the soluble portion by methods exactly analogous to those used for the hCCS proteins. When necessary, the protein was concentrated with an Amicon Centricon ultrafiltration cell. The purified protein contained one Zn ion per monomer and was presumed to be the E,Zn form. Fully metal loaded Cu,Zn-SOD was obtained by adding excess $CuSO_4$ to the E,Zn-SOD followed by exhaustive dialysis against Cu-free column buffer.

Cysteine and Selenocysteine Ligation, and Cu Reconstitution. The hCCS truncation mutant ending at amino acid 245 (CCS-245) was brought into the anaerobic chamber for selenocysteine ligation. We prepared 10 mM seleno-DL-cystine (Sigma) by dissolving it in a minimum volume of 6 M HCl, and then it was diluted to the correct volume brought with 50 mM sodium phosphate buffer (pH 7.2). The selenocystine was reduced with 20 mM tris(carboxyethyl)phosphine (TCEP) anaerobically. This solution was added to the hCCS mutant at a final concentration of 1 mM and incubated for 4 days in the anaerobic chamber with gentle shaking followed by exhaustive dialysis against Sec-free 50 mM sodium phosphate buffer (pH 7.2). Fully metal loaded Cys- or Sec-ligated proteins (245-Cys or 245-Sec) were obtained by reducing the ligated proteins over an immobilized TCEP disulfide reducing gel (Pierce Biotechnology, Inc.) and immediately adding a known amount of tetrakis(acetonitrile)copper(I) hexafluorophosphate [$Cu(MeCN)_4PF_6$] (Aldrich) dissolved in acetonitrile (MeCN) to the protein equilibrated in the same buffer containing 10% MeCN. The protein and Cu(I)/acetonitrile solution were left to sit for 1 h. This was followed by successive exhaustive dialyses against 5 and 0% MeCN in buffer to remove any free Cu(I) or MeCN. 245-Sec-ligated C22AC25A variants were prepared by analogous methods.

Protein and Metal Analysis. The protein concentration was measured by the Bradford assay. Copper was measured by inductively coupled plasma optical emission spectrometry (ICPOES) on a Perkin-Elmer Optima 2000 DV spectrometer. The oxidation state of the copper was determined by electron paramagnetic resonance spectroscopy (EPR) versus a Cu(II)-ethylenediaminetetraacetic acid (EDTA) standard on a Bruker Elexys 500 EPR spectrometer. The zinc concentration was measured by ICPOES spectrometry.

SOD1 Reconstitution Assays. The ability of hCCS to transfer copper to SOD1 was investigated by incubation of hCCS with E,Zn-SOD1 for variable times at 37 °C in a buffer of 50 mM sodium phosphate containing 10 μM bathocuproine sulfonate (BCS) and 10 μM EDTA at pH 7.8. The activity of the SOD1 was then measured by its ability to inhibit the reduction of cytochrome *c* by superoxide generated by the xanthine−xanthine oxidase reaction (*22*). An incubation time of 15 min was used unless otherwise stated.

XAS Data Collection and Analysis. Cu K-edge (8.980 keV) and Se K-edge (12.658 keV) extended X-ray absorption fine structure (EXAFS) data for the hCCS mutants were collected at the Stanford Synchrotron Radiation Laboratory operating at 3 GeV with currents between 100 and 75 mA. All samples were measured on beamline 9-3 by use of a Si[220] monochromator and a Rh-coated mirror upstream of the monochromator with a 13 keV (Cu) or 15 keV (Se) energy cutoff to reject harmonics. A second Rh mirror downstream of the monochromator was used to focus the beam. Data were collected in fluorescence mode on a high-count-rate Canberra 30-element Ge array detector with maximum count rates below 120 kHz. A 6 μm Z-1 metal oxide (Ni, As) filter and Soller slit assembly were placed in front of the detector to reduce the elastic scatter peak. Four to six scans of a sample containing only sample buffer [50 mM $NaPO_4$ (pH 7.2)] were collected at each absorption edge, averaged, and subtracted from the averaged data for the protein samples to remove Z-1 K_β fluorescence and produce a flat pre-edge baseline. This procedure allowed data with an excellent signal-to-noise ratio to be collected down to 100 μM total Cu or Se in the sample. The samples (80 μL) were measured as aqueous glasses (>20% ethylene glycol) at 10–15 K. Energy calibration was achieved by reference to the first inflection point of a copper metal foil (8980.3 eV) for Cu

K-edges and an elemental selenium foil (12658.0 eV) for Se K-edges, placed between the second and third ionization chamber. Data reduction and background subtraction were performed with the program modules of EXAFSPAK (*23*). Data from each detector channel were inspected for glitches or drop-outs before inclusion in the final average. Spectral simulation was carried out with EXCURVE 9.2 (*24–27*) as previously described (*13, 18, 28, 29*).

Mass Spectral Analysis. Protein masses were determined by electrospray ionization mass spectrometry. Proteins were injected onto a 0.3 mm × 10 mm C4 column (214MS53.10; Vydac), and masses were determined online using an ion trap (model LCQ Deca XP plus by Thermo Finnigan). The flow rate was 9 μL/min with a linear gradient from 2 to 75% MeCN over 55 min in a mobile phase containing 0.1% formic acid. Samples were injected using the Surveyor autosampler (Thermo Finnigan) and concentrated and/or purified using a protein micro trap cartridge (Michrom BioResources). Mass spectra of proteins eluted from the C-4 column were deconvoluted using BioWorks Browser (Themo Finnigan). A mass accuracy of better than 0.02% was confirmed using horse myoglobin.

RESULTS

Previous studies from our laboratory had established the presence of a Cu(I) cluster formed at the interface of two domain 3 polypeptides of the hCCS metallochaperone, with C244 and C246 of the D3 CXC motif as ligands to Cu(I) (*14*). Careful analysis of the XAS of WT protein and Cys to Ala mutants suggested that this cluster was multinuclear. Understanding the functional significance of this cluster in metal transfer and SOD1 maturation requires a more detailed knowledge of its composition. To this end, we set out to develop strategies for incorporation of selenium-containing amino acids into the cluster with the goal of using the Se XAS signal as a further probe of structure. Since the protein-derived ligands are Cys residues, our primary goal was to substitute selenocysteine (U) for cysteine and generate 243-UAC and 243-CAU sequences at positions 244–246. We chose the method of expressed protein ligation (*30–32*) which we had used with success previously to substitute Sec and Sem (selenomethionine) into azurin (*21, 33*). In the azurin case, U was incorporated into an 11-mer oligopeptide which was ligated to a truncated C-terminus, thereby generating a functional protein with native spectroscopic features. In the case presented here, the strategy would involve ligation of an oligopeptide with either C(U)244 or C(U)246 as the N-terminal residue. In our previous studies on WT hCCS, we had used a fully active construct missing the last five amino acids and terminating at residue 268. Semisynthesis of this protein by expressed protein ligation would require coupling of a 25-mer Sec-containing synthetic peptide to the CCS-243 truncation. Since the peptide synthesis and ligation yield both become increasingly challenging with increasing lengths of oligopeptides, our first step was to discover the shortest C-terminus that would allow retention of metal transfer activity.

Nomenclature. hCCS variants are named as follows. Truncated proteins are represented by CCS-*n*, where *n* is the residue number of the C-terminal residue. Cys- and Sec-ligated proteins are designated 245-Cys and 245-Sec, respectively, which correspond to ligation of Cys and Sec to the truncation terminating at residue 245. The C-terminal sequences for these ligated proteins were $C^{244}AC^{246}$ and $C^{244}AU^{246}$, respectively.[2]

Table 1: Metal Transfer Activities of hCCS C-Terminal Truncation Mutants and the CCS245Cys and CCS245Sec Variants Prepared by Expressed Protein Ligation of Cys or Sec to the CCS245 Truncation

sample	activity[a] (units)
Cu,Zn-SOD1	2000
hCCS	1500
CCS246	1282
CCS247	1326
CCS252	1238
CCS245Cys	1042
CCS245Sec	1006

[a] Copper transfer activity was measured as the ability of hCCS to activate apo-SOD1 as determined from the inhibition by SOD1 of the xanthine−xanthine oxidase coupled reduction of cytochrome *c*. The assay was normalized by setting the activity of SOD1 reconstituted by $CuSO_4$ to an arbitrary value of 2000 units. All hCCS activities are standardized to this value.

Plasmid-Based Expression of Truncated Proteins. We created truncated versions of hCCS after Cys246, Asp247, and Tryp252 (CCS-246, CCS-247, and CCS-252, respectively) by PCR amplification of wild-type hCCS and measured their activity. DNA sequences were ligated into the pTXB-3 intein-containing plasmid and overexpressed in *E. coli* ER2566 with IPTG and zinc addition. After purification on chitin beads and intein cleavage, the truncation mutants were analyzed for activity and metal content by ICPOES. Typically, all of the proteins bound one Zn per mole of protein such that copper binding stoichiometries could be determined from the Zn:Cu ratios. Copper reconstitution was performed anaerobically by addition of a 3-fold excess of $Cu(MeCN)_4^+$ followed by dialysis to remove remaining free copper and acetonitrile. CCS-246 bound 2.3 Cu/Zn, CCS-247 2.7 Cu/Zn, and CCS-252 2.4 Cu/Zn per monomer. Activity was assayed by measuring the ability of the truncation mutants to transfer copper to apo-SOD1, and the results are listed in Table 1 and Figure 2. As reported previously (*13*), the amount of SOD1 activity recovered by reconstitution of E,Zn-SOD with hCCS (1500 units) is smaller than the amount of E,Zn-SOD reconstituted with inorganic cupric ions (2000 units). However, the activities of the 246, 247, and 252 truncation mutants were the same within experimental error, and ~90% of the WT hCCS activity. Further analysis of the time course of SOD1 activation (Figure 2) suggested that activity levels close to that of the Cu^{2+}-reconstituted SOD could be achieved by increasing the time of incubation. Therefore, while the CXC motif is essential for inducing SOD activation, the additional C-terminal sequence is not required but may accelerate the metal transfer.

Semisynthesis of 245-Cys and 245-Sec. Since the CXC motif was both necessary and sufficient for SOD maturation, we chose initially to create a CAU motif as the C-terminal sequence since this could be achieved by ligating a single selenocysteine onto the CCS-245 truncation mutant. Thus, a ^{245}Ala truncation mutant, where Ser245 was mutated to an Ala for more efficient ligation, was created by PCR

[2] Residue 245 was mutated from the native serine to alanine for more efficient ligation (vide infra).

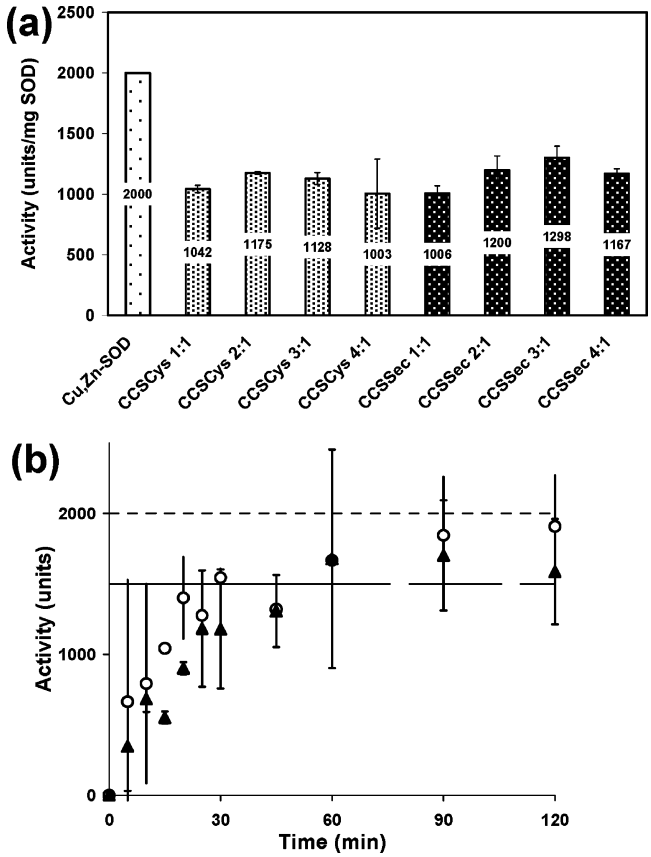

FIGURE 2: (a) Activities of hCCS 245-Cys and 245-Sec as a function of CCS:SOD1 ratio. (b) Time course of SOD1 activation by CCS-246 (○) and 245-Sec (▲). The horizontal dashed line represents the activity of the $CuSO_4$-reconstituted SOD1, and the horizontal solid line represents the activity of full-length (residues 2–269) WT hCCS.

amplification of hCCS. The CCS-245 truncation was then expressed in *E. coli* ER2566 and purified on a chitin column with intein cleavage by mercaptoethanesulfonic acid (MESNA). Single-amino acid ligation of selenocysteine or cysteine (as a control) to the truncated protein was performed anaerobically. Seleno-DL-cystine was first reduced with TCEP and then added in a 1:10 ratio (protein:Sec) to the truncated protein. After anaerobic incubation for 4 days, free selenocysteine and TCEP were removed by dialysis. Successful ligation was confirmed by ICP analysis of zinc and selenium concentrations and by mass spectrometry analysis. Cys ligation was performed in a similar fashion.

Copper Reconstitution. Reconstitution of the newly synthesized protein with Cu(I) posed a challenge. 245-Sec was extremely sensitive to diselenide formation even under anaerobic conditions, thereby preventing binding of Cu(I) to the CAU motif. To circumvent the tendency toward oxidation, it was necessary to reduce the diselenide with tricarboxyethylphosphine (TCEP) followed by rapid addition of the Cu(I) under anaerobic conditions. This was most conveniently achieved by use of an immobilized TCEP reducing column, where immobilization of the phosphine reductant precluded its presence in a soluble form which could coordinate to Cu(I) (*29*). Protein was added to the TCEP-bound agarose in a column and left to reduce for 1 h. After elution with 2 volumes of buffer, 3 molar equiv of $Cu(I)(MeCN)_4^+$ in acetonitrile was immediately added to the protein. Reconstituted proteins were then dialyzed against decreasing amounts of acetonitrile in 50 mM phosphate buffer to remove free copper and acetonitrile. Metal analysis by ICPOES (Table 2) showed that the concentrations of Cu, Zn, and Se in hCCS 245-Sec were 900, 400, and 409 μM, respectively. Thus, the 245-Sec protein bound one Se per Zn, indicating efficient Sec ligation, and 2.2 Cu per Zn and Se.

Ligation Efficiency. Mass spectral data give an independent estimate of the efficiency of the ligation process. Figure 3 shows the mass spectral data for Cys and Sec ligations. The mass for the Cys-ligated (*m*/*z* 25837) protein is the expected mass for 245-Cys with two disulfide cross-links and the N-terminal methionine residue cleaved (*m*/*z* calcd 25837). The two disulfides probably correspond to the C141−C227 disulfide observed in the hCCS D2 crystal structure and a C22−C25 disulfide which is seen in the apo-yCCS structure. The Sec-ligated protein exhibits an intense peak at *m*/*z* 25880. The mass corresponding to the analogous Sec-substituted protein with Met1 cleaved and two disulfides is *m*/*z* 28884. This suggests that at least one additional S−S or Se−S bond exists in the Sec protein and is consistent with formation of a S−Se bond between C244 and U246 of the D3 CXU motif. Peaks representing the unligated protein in the Sec-ligated spectrum appear to be absent, although they may be present at low levels.[3] The low-intensity peak in the Cys-ligated spectrum at *m*/*z* 25663 does not correspond to unligated CCS-245 truncation (*m*/*z* calcd 25737, +MESNA *m*/*z* 26248) but could represent a truncated protein terminating at C244 with the Ala^{245} cleaved (*m*/*z* calcd 25662). The absence of any species with a mass representative of the CCS-245 truncated starting material suggests close to 100% efficiency of the ligation process.

SOD1 Activation by Semisynthetic 245-Cys and 245-Sec. Both ligation constructs were assayed for activity by measuring their ability to transfer copper with a 30 min incubation time to apo-E,Zn-SOD1 at a hCCS:SOD1 ratio of 1:1 (Table 1). Both Cys and Sec-ligated proteins had the same transfer activity within experimental error but appeared to have a slightly lower activity than the plasmid-expressed controls. The cysteine-ligated hCCS retained 81% of its activity, whereas the selenocysteine-ligated protein retained 78% compared to plasmid-expressed CCS-246. The slightly decreased activity of the ligation mutants could be due to (a) <100% ligation efficiency or (b) slower transfer kinetics. Since the Se:Zn ratio was unity, and mass spectrometric analysis indicated no observable unligated CCS-245 truncated precursor, the former explanation seems unlikely. Panels a and b of Figure 2 show the effect on activity of (a) increasing the CCS:SOD1 ratio and (b) increasing the reaction time. Both lead to increased transfer activity, suggesting that slower transfer kinetics are the likely origin of the decreased activity of the 245-Cys/Sec ligated proteins. It is clear, however, that substitution of Se for S has no effect on the SOD1 maturation activity.

Spectral Characterization of Apo-245-Sec. With selenocysteine covalently attached to hCCS as the C-terminal residue, it was possible to probe the speciation of the Se by

[3] For example, a minor component of unligated protein (<10%) with a cross-link between C244 and a free selenocysteine amino acid would probably be undetectable in the mass spectrum yet would still be assesed as having one Se per monomer.

Table 2: Metrical Details Derived from Cu and Se EXAFS of the Cu(I)-Loaded CCS245Cys and CCS245Sec Variants Prepared by Expressed Protein Ligation of Cys or Sec to a CCS245 Truncation[a]

		metal content[c]		first shell			second shell			
sample	F^b	[metal] (μM)	[M]/[P]	no.[d]	R (Å)[e]	DW (Å^2)	no.[d]	R (Å)[e]	DW (Å^2)	$-E_0$[f]
				Cu-XAS						
CCS246	0.380	[Cu] = 1070, [Zn] = 485	2.2	3.0 S	2.24	0.007	1.0 Cu	2.69	0.021	4.24
CCS245Cys	0.372	[Cu] = 1100, [Zn] = 574	1.9	3.0 S	2.24	0.006	1.0 Cu	2.71	0.011	4.12
CCS245Sec	0.241	[Cu] = 900, [Zn] = 400, [Se] = 409	2.2	2.0 S 0.8 Se	2.23 2.40	0.005 0.007	1.4 Cu	2.70	0.013	3.06
C22AC25A-245Sec	0.359	[Cu] = 1000, [Zn] = 550, [Se] = 550	1.8	2.0 S 1.1 Se	2.22 2.41	0.005 0.007	2.9 Cu	2.70	0.012	2.34
				Se-XAS						
CCS245Sec PreTCEP	0.340	[Zn] = 860, [Se] = 900	1.0	1.0 C	1.99	0.006	0.26 S 0.74 Se	2.21 2.32	0.006 0.006	6.28
CCS245Sec	0.242	[Cu] = 900, [Zn] = 400, [Se] = 409	1.0	1.0 C	1.99	0.005	2.0 Cu	2.38	0.007	4.66
C22AC25A-245Sec	0.272	[Cu] = 1000, [Zn] = 550, [Se] = 550	1.0	1.0 C	1.99	0.005	2.0 Cu	2.38	0.007	1.18

[a] Fits were obtained by curve fitting using EXCURV version 9.2. [b] F is a least-squares fitting parameter defined in ref *14*. [c] [M]/[P] represents the metal to protein ratio of the absorption edge being analyzed. Cu and Se to protein ratios are calculated assuming hCCS binds one Zn per monomer. [d] Coordination numbers are generally considered accurate to ±25%. [e] In any one fit, the statistical error in bond lengths is ±0.005 Å. However, when errors due to imperfect background subtraction, phase-shift calculations, and noise in the data are compounded, the actual error is probably closer to ±0.02 Å. [f] E_0 is a small correction to the experimental energy threshold ($k = 0$) which was set to 8985 eV for Cu EXAFS and 12663 for Se EXAFS.

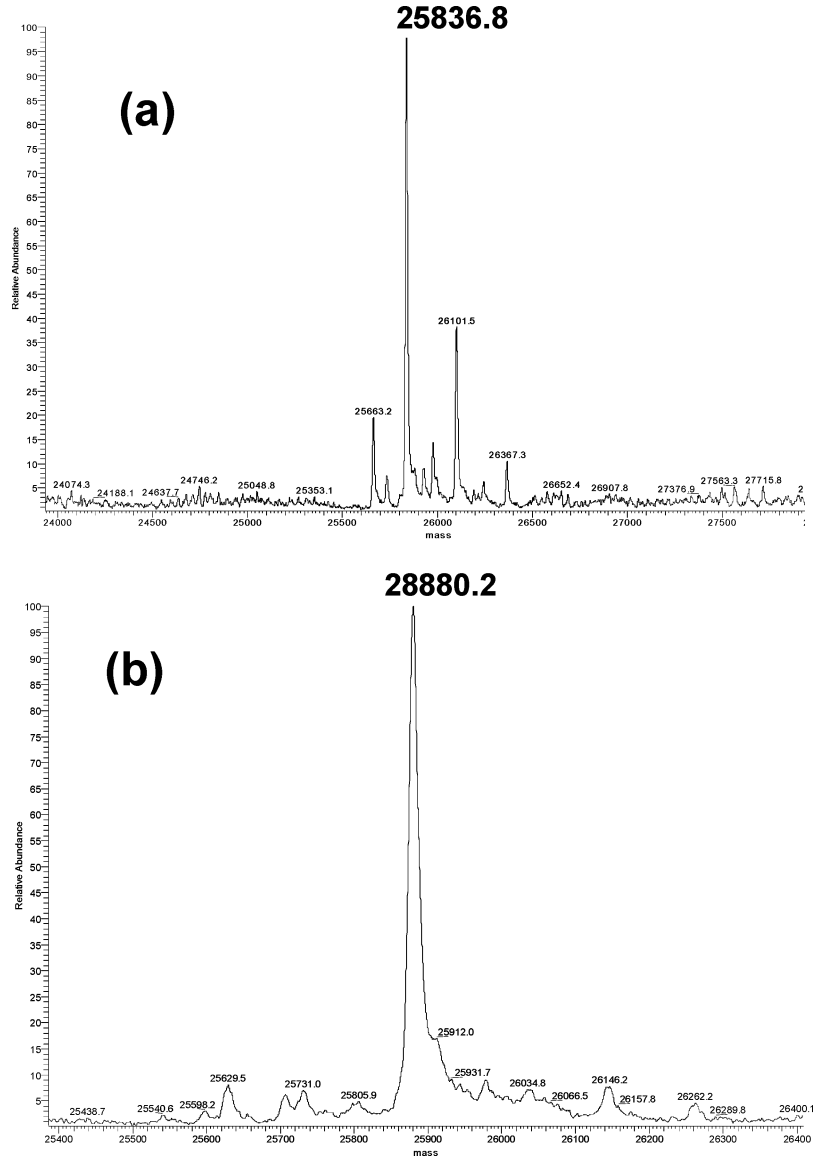

FIGURE 3: Electrospray ionization mass spectrum of (a) hCCS 245-Cys and (b) hCCS 245-Sec.

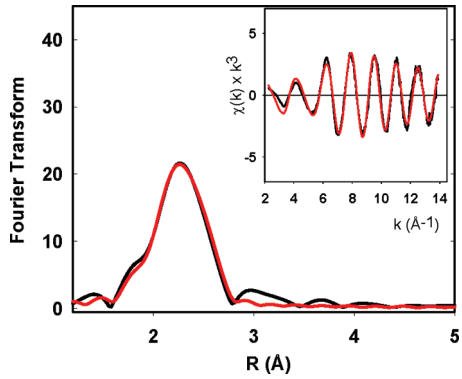

FIGURE 4: Fourier transform and EXAFS (inset) at the Se K-edge for hCCS 245-Sec immediately after ligation, prior to reduction by TCEP. Black lines show experimental data, and red lines show simulated data. Parameters used in the fit are listed in Table 2.

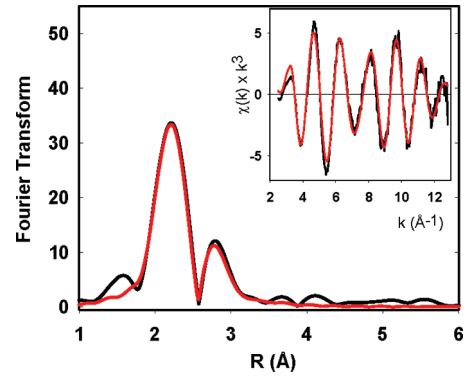

FIGURE 5: Fourier transform and EXAFS (inset) at the Cu K edge for hCCS 245-Cys. Black lines are experimental data, red lines are simulated data. Parameters used in the fit are listed in Table 2.

Se K-edge EXAFS. A number of structural environments were possible. First, the Se could be present as a reduced selenol or selenide which would result in predominant Se−C first-shell scattering. Alternatively, as suggested by the mass spectral data, oxidation could lead to a selenylsulfide (S−Se), in which case a Se−S bond would accompany the Se−C interactions in the first shell. Finally, a Se−Se interaction might occur if CAU motifs from two domain 3 polypeptides could cross-link. This latter situation would be reminiscent of the Cu(I) cluster formation that we have shown to occur at a domain 3−domain 3 dimer interface (*13, 14*). EXAFS spectra for apo-245-Sec prior to TCEP reduction are shown in Figure 4. Fits using either a Se−C bond or a mixed Se−C/Se−S bond were unable to reproduce the increase in amplitude of the EXAFS oscillations maximizing at a k of ~9 Å^{-1}. This pattern of EXAFS amplitude envelope is typical of scattering from heavy atoms such as transition metals and heavier chalcogenides. Therefore, we also considered fits with Se−Se interactions arising from domain 3 dimerization. The best fit was found to be a mixture of both Se−S (0.3) and Se−Se (0.7) bonds with an F value of 0.340 (Table 2). This shows that as isolated, the ligated protein appears to be oxidized and exists as an equilibrium mixture of monomers with Se−S distances of 2.21 Å and dimers with Se−Se distances of 2.32 Å. These results emphasized the need for reduction of the ligated proteins on the immobilized TCEP column prior to reconstitution with Cu(I). Se EXAFS was also used to probe the Se oxidation state after this TCEP reduction step, but the data could not be interpreted in terms of a simple model such as a single Se−C shell as expected for a reduced selenol. The reasons for the complexity of the Se EXAFS after reduction are unclear (since all steps were performed anaerobically), but it is possible that further reaction and/or oxidation might have occurred during the time taken to concentrate the samples for XAS analysis. This aspect of apo-245-Sec chemistry was not explored further.

X-ray Absorption of Cu(I)-Bound 245-Cys and 245-Sec Proteins. 245-Cys (CAC) Cu Edge. Cu K-edge EXAFS of the Cys-ligated hCCS are shown in Figure 5. As expected the 245-Cys protein is very similar to the previously reported XAS of the WT protein (untagged, residues 1–268, (*14*)). Two shells of scatterers are observed at ~2.2 and 2.7 Å, corresponding to Cu−S and Cu−Cu respectively. Curve fitting analysis leads to a best fit with 3 Cu−S interactions (R, $2\sigma^2$) at 2.24 Å (0.006 Å^2) and 1 Cu−Cu at 2.71 Å (0.011 Å^2). From previous work on the C22AC25A double mutant constructed in the full length (untagged) protein, it was concluded that a multinuclear Cu(I) cluster was formed at the interface of two D3 polypeptides, with a characteristic DW of 0.012 Å^2 for the Cu−Cu interaction (*14*). Since both D1 and D3 Cu binding sites are presumed to be occupied in a 1:1 ratio, this would equate to 2 Cu−Cu interactions per Cu center in the D3 cluster, or a nuclearity ≥3.

245-Sec (CAU) Se Edge. For the Sec-ligated protein, the Se edge data were analyzed first, as Se is present only in D3, and hence, Se XAS would report only on the D3 cluster without any contribution from the D1 site. The Se EXAFS should contain contributions from one Se−C bond and a number of Se−Cu interactions, depending on the structural composition of the cluster. As expected, the data show strong contributions from a heavy atom scatterer maximizing at a k of ~9 Å^{-1}. Simulations were attempted with one Se−C bond and an adjustable number of Se−Cu interactions. A single Se−Cu interaction gave an F value of 0.507 with Se−C and Se−Cu bond lengths [$R(2\sigma^2)$] of 2.01 Å (0.002 Å^2) and 2.38 Å (0.001 Å^2), respectively. In this fit, the EXAFS amplitude was not adequately fit even with the extremely low Se−Cu DW factor. A much improved fit, where $F = 0.242$ (Figure 6, bottom trace), was obtained with one Se−C and two Se−Cu interactions with an $R(2\sigma^2)_{Se-C}$ of 1.99 Å (0.005 Å^2) and an $R(2\sigma^2)_{Se-Cu}$ of 2.38 Å (0.007 Å^2). When the Se−Cu occupation number and DW were allowed to float freely, the Se−Cu coordination number refined to 1.9 ($2\sigma^2 = 0.006$ Å^2).[4] These simulations suggest that each Se is bound by two Cu atoms at 2.38 Å in the D3 cluster. The small doublet at k = 2–3 was best fit by including a Se−S shell at 3.98 Å and may represent interactions with more distant S atoms within the multinuclear cluster. (Because of the high uncertainty associated with these outer shell interactions, their metrical details have been excluded from Table 2.)

245-Sec (CAU) Cu EXAFS. The analysis of the Cu EXAFS is more complex, as it represents the average of the Cu binding to the D1 mononuclear site and the D3 multinuclear site. However, the Se−Cu metrical data extracted from the

[4] The shell occupation number and DW factor are highly correlated, and consequently, this procedure does not necessarily lead to the "best fit". However, it is a useful way of validating the conclusions of more stringent fitting protocols which generate minima under conditions where only noncorrelated variables float.

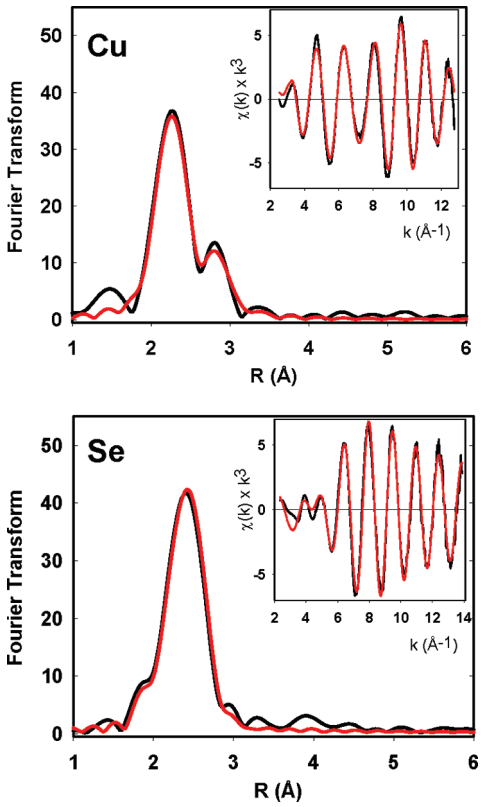

FIGURE 6: Fourier transform and EXAFS (inset) for hCCS 245-Sec: top trace, Cu K-edge data; bottom trace, Se K-edge data. Black lines show experimental data, and red lines show simulated data. Parameters used in the fit are listed in Table 2.

Se EXAFS analysis provide an accurate (±0.02 Å) Se−Cu distance and DW factor as an input to the analysis of the Cu EXAFS, and (as before) we can set the Cu−Cu DW to 0.012 Å^2. These "hard" input parameters allowed other Cu−ligand interactions to be more accurately determined. With Cu bound at D1 in a predominately Cu−S environment and the expected coordination of C244 from each D3 polypeptide, analysis of the Cu EXAFS was carried out with Cu−S, Cu−Se, and Cu−Cu shells. The best fit (Figure 6), top trace using a Cu−Se distance of 2.38 ± 0.02 Å and a $2\sigma^2$(Cu−Cu) of 0.012 Å^2, gave 2.2 Cu−S bonds at 2.24 Å (0.010 Å^2), 0.7 Cu−Se bond at 2.40 Å (0.007 Å^2), and 1.4 Cu−Cu bonds at 2.71 Å (0.012 Å^2). These parameters lead to full consistency of metrical parameters at both Cu and Se absorption edges.

C22AC25A CCS-245-Sec. The presence of Cu bound to domain 1 complicates the interpretation of the Cu XAS data since the EXAFS represents the average of Cu−ligand scattering at both the D1 and D3 sites. To overcome this difficulty, we synthesized the 245-Sec derivative in the C22AC25A double mutant variant. As noted above, previous studies on this variant in a nontruncated form (terminating at residue 268), with residue 246 being a cysteine (*14*), suggested a multinuclear cluster linking two D3 polypeptides, with no contributions from any other Cu center. Careful analysis of the magnitude of the Cu−Cu Debye–Waller factors in this and other published Cu_xS_y clusters led to the conclusion that a Cu_4S_6 adamantane-type cluster was most consistent with the data. It should be straightforward to test the structural model, by assessing the effect of substitution of two Se atoms for S to generate a $Cu_4S_4Se_2$ cluster.

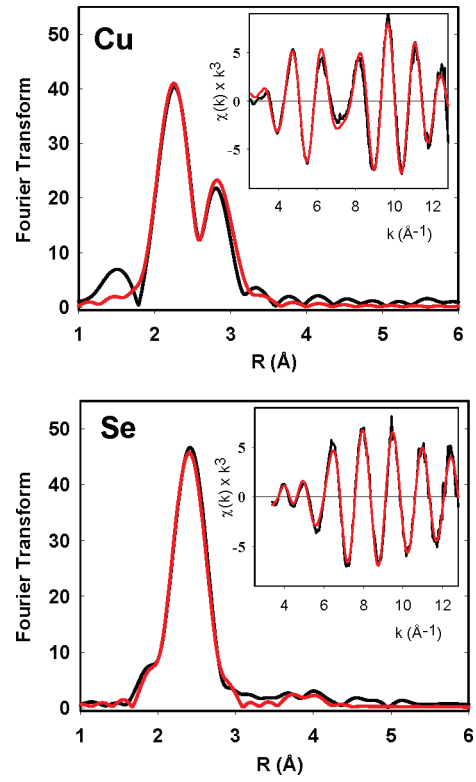

FIGURE 7: Fourier transform and EXAFS (inset) for hCCS C22AC25A 245-Sec: top trace, Cu K-edge data; bottom trace, Se K-edge data. Black lines show experimental data, and red lines show simulated data. Parameters used in the fit are listed in Table 2.

C22AC25A CCS-245-Sec was prepared by ligation of selenocysteine to the C22AC25A CCS-245 truncation by methods analogous to those used for the WT protein. Mass spectrometry identified a peak at *m/z* 25817. The calculated mass with Met1 cleaved and the two native disulfides is *m/z* 25819. This suggests that like the WT Sec-substituted protein, one additional S−S or Se−S bond exists in the monomeric protein and is again consistent with formation of a seleno-sulfide bond between C244 and U246 of the D3 motif. EXAFS studies on the apo-Sec-ligated double mutant (data not shown) confirmed the presence of an equilibrium mixture of Se−S (0.4, 2.21 Å) and Se−Se (0.6, 2.32 Å) interactions. After concentration for XAS, the Cu, Zn, and Se concentrations were found to be 1000, 550, and 550 μM, respectively, corresponding to a Cu:Se ratio of 1.8:1. The absence of significant peaks due to unligated 245 truncation and the 1:1 Se:Zn ratio suggested ligation efficiencies close to 100%.

Figure 7 (bottom) shows the Se and Cu EXAFS for C22AC25A CCS-245-Sec. The Se EXAFS is qualitatively and quantitatively identical to that of the WT CCS-245-Sec derivative, yielding values of one Se−C bond at 1.985 Å and two Se−Cu bonds at 2.381 Å. As for the WT data, the small doublet at k = 2–3 was best fit by including a Se−S shell at 3.98 Å and may represent interactions with more distant S atoms within the multinuclear cluster.

Figure 7 (top) shows the analogous Cu EXAFS for the C22AC25A CCS-245-Sec protein. Previous analysis of C22AC25A CCS-268, for which only Cu XAS data were available, used the average (0.012 Å^2) DW factors from eight multinuclear Cu(I) clusters to predict a cluster nuclearity between 3 and 4 (*14*). Applying the same analysis to the data presented here (including restraints that Cu−Se bond

lengths and DW factors must be the same within experimental error) leads to a best fit with metrical parameters [R ($2\sigma^2$)] of 2.0 Cu−S bonds at 2.22 Å (0.005 Å^2), 1.1 Cu−Se bonds at 2.41 Å (0.007 Å^2), and 2.9 Cu−Cu interactions at 2.70 Å (0.012 Å^2).

Alternative Fits. The apoprotein prior to reduction contained S−Se and Se−Se cross-links, and our efforts to demonstrate the presence of the selenol after reduction were unsuccessful. Specifically, EXAFS data at the Se edge on concentrated samples of the TCEP-reduced apoprotein still showed the presence of Se−Se interactions. Since it took a significant period of time to concentrate the samples, we suggested that the samples reoxidized during concentration. By contrast, Cu(I) reconstitution was performed immediately after the apoprotein sample emerged from the TCEP reducing column and was thus expected to lead to optimal amounts of selenolate−Cu(I) coordination. Notwithstanding, we cannot eliminate the possibility that some Se−Se cross-linked hCCS molecules coexist with the Cu(I)-bound selenolato-CCS. The situation is compounded by the fact that Se−Cu and Se−Se interactions are potentially hard to distinguish by EXAFS simulation, since Cu and Se are separated by only four elements in the third row of the periodic table.

To address this question, we carried out simulations of the Cu and Se EXAFS spectra of the C22A25A 245-Sec derivative in which both Se−Se and Se−Cu interactions were included. Fitting the Se EXAFS data with one Se−C and one Se−Se cross-link, the situation expected if all of the 245Sec protein were present as a diselenide-bridged dimer with no Cu(I) coordination, gave a poor fit ($F = 0.89$ vs the best fit value for two Cu−Se interactions of 0.27) and was inconsistent with the Cu:protein binding ratio of two Cu atoms per Se and the Cu EXAFS which, as demonstrated above, showed the presence of a multinuclear cluster. Fits to the Se data which allowed for the presence of both Se−Se and Se−Cu interactions were more successful. We searched parameter space for acceptable fits to the Se EXAFS data by floating the occupation numbers of the Se−Cu and Se−Se EXAFS components for a series of pairs of Se−Cu and Se−Se distances. The Debye–Waller terms for the Se−Cu and Se−Se shells were fixed at appropriate values of 0.007 and 0.006 A^2, respectively.[5] A further constraint was imposed; the maximum Se−Se occupation number could not exceed 1, corresponding to a Se−Se interaction between Se atoms in each of two polypeptide chains. For each pair of distances, a three-dimensional map of the surface was constructed by plotting N_{Se-Cu} and N_{Se-Cu} as x- and y-coordinates, respectively, and F (or $1/F$) as the z-coordinate. The results of this analysis are listed in Table S1 of the Supporting Information. Two minima with acceptable F values ($F < 0.4$; $1/F > 2.5$) were discovered and are shown as contour maps in Figure 8. These correspond to the fit described above with two Cu−Se bonds at 2.38 Å with no Se−Se interaction and an additional model with 2 ± 0.5

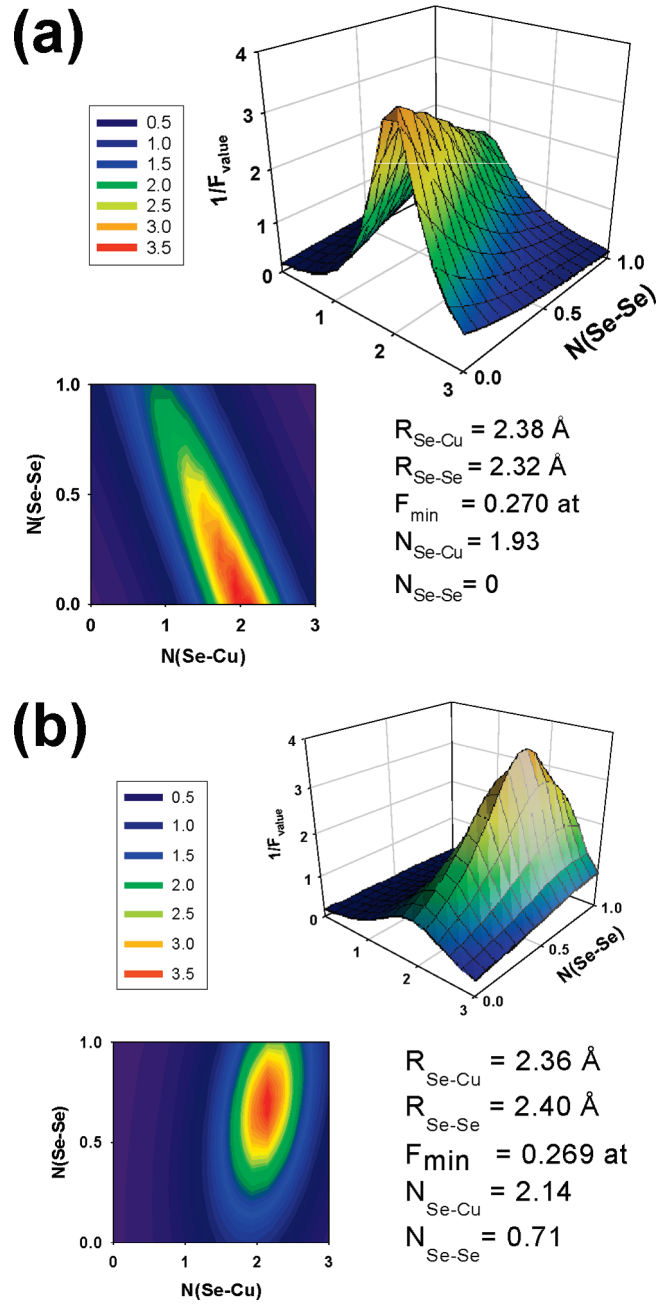

FIGURE 8: Two acceptable minima of the least-squares residual F in a search of parameter space of the Se EXAFS of C22AC25A CCS245Sec. The minima in F are illustrated by three-dimensional contour maps of the minimization surface constructed by plotting N_{Se-Cu} and N_{Se-Cu} as x- and y-coordinates, respectively, and $1/F$ as the z-coordinate such that the best fits appear as maxima in the plots: (a) surface obtained with no Se−Se component and (b) surface showing the unique minimum at two Cu−Se bonds at 2.36 Å and 0.7 Se−Se bond at 2.40 Å. The analysis was carried out by floating the occupation numbers of the Se−Cu and Se−Se EXAFS components for a series of pairs of Se−Cu (2.34–2.44 Å) and Se−Se (2.30–2.44 Å) distances. The Debye–Waller terms for the Se−Cu and Se−Se shells were fixed at appropriate values of 0.007 and 0.006 Å^2, respectively (see footnote [5]). A further constraint was imposed; the maximum Se−Se occupation number could not exceed 1, corresponding to a Se−Se interaction between Se atoms in each of two polypeptide chains.

[5] Since occupation numbers and DW factors are highly correlated, it was necessary to fix the Debye–Waller factors to obtain meaningful results. The value of 0.007 Å^2 for the Se−Cu Debye–Waller factor ($2\sigma^2$) was chosen from the value obtained in fits to the Se EXAFS of Cu(I)-reconstituted CCS245Sec with two Se−Cu interactions and no Se−Se interactions (Table 2). This value is reasonable as it lies within the range (0.003–0.015 Å^2) of Se−Cu DW factors found for Sec112 azurin (*44*) and selenomethionine Cu_A (*57*) with Se−Cu distances of 2.31 and 2.55 Å, respectively, and is also close to that observed in a selenomethionine derivative of CusF (unpublished work). The value of 0.006 Å^2 for the Se−Cu Debye–Waller factor ($2\sigma^2$) was chosen from the value obtained from the Se−Se interaction in fits to the Se EXAFS of apo CCS 245Sec.

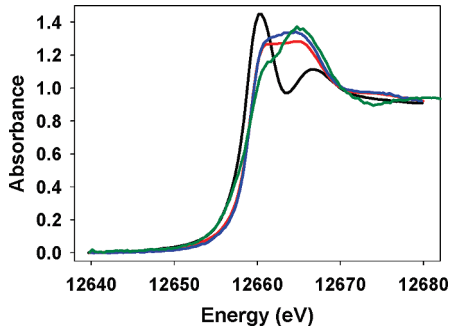

FIGURE 9: Se K-absorption edges for selenocysteine−protein complexes: black trace, apo hCCS-245-Sec as isolated prior to TCEP reduction (containing Se−S and Se−S interactions); red trace, Cu(I)-reconstituted WT CCS-245-Sec; blue trace, Cu(I)-reconstituted C22AC25A CCS-245-Sec; and green trace, Cu(I)-112Sec azurin from ref *21*. Edge intensities are normalized at 12670 eV.

Cu−Se bonds at 2.36 Å, and 0.7 ± 0.1 Se−Se bond at 2.40 Å. The latter scenario would model the situation in which a fraction of the protein remained as the oxidized diselenide form [unavailable for Cu(I) coordination] while the remainder participated in cluster formation. Alternatively, Se−Se bonds could exist within the multinuclear cluster.

Figure 9 shows Se K-absorption edges for apo CCS-245Sec, and the Cu(I)-reconstituted 245-Sec of the WT and C22AC25A variant. The edge profile of the apoprotein contains a pair of peaks at 12660.5 and 12666.5 eV with an intensity ratio of 1.3. These peaks closely resemble the profiles for oxidized selenocysteine containing either Se−S or Se−Se bonds as reported by Pickering and co-workers (*34*) and are fully consistent with our assignment as mixtures of selenosulfide and diselenide isoforms. Cluster formation by Cu(I) metalation leads to changes in the edge profiles. The edges of the WT and C22AC25A variants are similar (as expected) and exhibit a broad unresolved feature maximizing between 12662.5 and 12665 eV. This band most likely can be assigned to the same transitions as for the apoprotein (1s → σ^* for Se−S/Se, and 1s → σ^* for Se−C), but with modified energies and intensities due to the effects of mixing with Cu(I) 4s and 4p levels. Also shown is a comparison with the Se K-edge of the Cu(I) derivative of Sec112 azurin which contains a mononuclear Cu(I)−selenolate bond (*21*). The azurin spectrum exhibits peaks at the same energies as for Cu(I)−CCS-245Sec, but with different intensity ratios, implying that the multinuclear cluster has a unique electronic structure. The presence of two Cu−Se bonds and/or the lengthening of the Cu−Se bond from 2.31 Å in Sec112 azurin to 2.38 Å in Sec-CCS is the likely origin of this effect. Copper edges were not notable, being entirely typical of three-coordinate Cu(I), and were changed little from those reported earlier for the WT and C22AC25A cysteine-containing proteins. The Cu edges of the CCS-245Sec and its C22AC25A variant are given in Figure S1 of the Supporting Information.

DISCUSSION

We have reported the semisynthesis of a selenocysteine derivative of the human copper chaperone for superoxide dismutase, substituted with Sec at the C-terminal C246 residue. Measurements of hCCS-induced SOD1 activation have shown that this sequence is both necessary and sufficient for E,Zn-SOD maturation such that the formation of the Sec derivative could be achieved by expressed protein ligation of a single selenocysteine amino acid to a CCS-245 truncation. This reaction proceeded in high yield and generated the desired 245-X (X = C or U) protein of the expected mass, using both Cys and Sec. On the basis of previous findings, the CAU sequence should contribute to the multinuclear Cu(I) cluster which forms at the domain 3 interface of a hCCS dimer. Thus, the Sec-ligated protein contains both Cu and Se as constituent atoms of the cluster and should provide additional details about the cluster structure through merging of XAS data at the Cu and Se K-absorption edges.

Although Sec has been discovered in an increasing number of proteins as the "21st" amino acid, biological Sec incorporation is a complex and highly specialized process (*35, 36*). In eukaryotes, a special mRNA stem−loop sequence (SECIS) is inserted into the 3′-untranslated region which directs UGA to be interpreted as Sec rather than STOP and requires the presence of a number of accessory proteins. In prokaryotic systems, however, the SECIS element is found immediately downstream of the UGA codon and is part of the open reading frame. This severely restricts the utility of SECIS elements in the overexpression of Sec-containing protein variants, unless the Cys to Sec mutation is at or very close to the C-terminus since the SECIS element is translated. The necessity of simultaneously overexpressing the accessory proteins adds further complexity. Using this approach, successful incorporation of a Sec-substituted thioredoxin was reported by Arner and co-workers (*37*), but only 50% Sec incorporation was obtained, which necessitated the development of affinity methods for separating Sec from Cys variants (*38*).

Greater success has been achieved using the technique of expressed protein ligation (EPL) (*30–32*), where synthetic peptides with C-terminal Cys residues react with peptides carrying a thioester moiety at a C-terminal truncation to generate a native peptide bond. EPL-mediated Sec derivatives were successfully prepared in ribonuclease (*39*), azurin (*21, 40*), and thioredoxin reductase (*41*). In related studies, native pepide ligation was used to generate Sec derivatives of bovine pancreatic trypsin inhibitor (*42*) and a C-terminal 17-mer fragment of ribonucleotide reductase (*43*). A more complex approach was used to synthesize Sec-substituted glutaredoxin using two synthetic oligopeptides, an N-terminal 37-mer substituting Sec for each Cys of the CXXC motif and a C-terminal 44-mer carrying an engineered Cys residue at its N-terminus for coupling (*44*) .

The Sec-substituted hCCS synthesized in this work was found to be present in forms containing both Se−S and Se−Se cross-links. The Se−S selenylsulfido form could represent either intramolecular cross-linking between C244 and U246 or intermolecular dimerization. Given the precedent for intramolecular Se−S formation in selenoenzymes (*45–47*), we propose that the former scenario is more likely. However, the Se−Se interaction clearly identified in the Se-EXAFS of the apoprotein can arise only from an intermolecular diselenide formed via dimerization of the domain 3 polypeptide. This feature of Sec-hCCS is of great interest since it mimics the formation of the D3−D3 dimer induced by Cu(I) cluster formation and, thus, suggests that D3 dimerization involves favorable protein–protein interactions. On the other hand, comparisons of the redox potential of disulfides,

selenylsulfides, and diselenides clearly show a decrease in potential throughout the series, providing an alternative driving force for the D3−D3 diselenide cross-link. For disulfides, the potentials span a range from −124 V for the bacterial protein-folding factor DsbA to −270 mV in thioredoxin (*48*). Data for selenylsulfides and diselenides are less abundant, but a recent study of Sec-substituted glutaredoxin-3 reports values of −260, −275, and −309 mV for the C11U, C14U, and C11U/C14U variants, respectively, compared with a value of −194 mV for the native CXXC protein (*44*). Similarly, the redox potential of a selenylsulfide measured in a synthetic octapeptide (−326 mV) is ∼60 mV more positive than that of its diselenide derivative (approximately −390 mV) (*49*). The newly discovered selenoprotein Sep15 contains a CXU motif in mammalian isoforms and, thus, most closely resembles the CXU motif of Sec-hCCS (*50*). These studies emphasize the stronger tendency toward diselenide formation in selenoproteins and their catalytic intermediates.

Sec-substituted hCCS binds 2−2.5 molar equiv of Cu(I) and has activity in SOD1 activation equivalent to that of its S-containing homologue. The consistent increase in Cu:CCS monomer ratios above 2.0 suggests that the D3−D3 cluster has a nuclearity greater than 2. X-ray absorption measurements at the Cu and Se K-edges have been analyzed to provide metrical details of the coordination environments of the Cu and Se atoms, and by necessity, Cu−Se and Se−Cu interactions determined from the Cu and Se data sets must have identical coordination numbers, bond lengths, and DW factors. This introduces constraints into the fitting analysis which should produce a more accurate picture of the multinuclear Cu(I) cluster, and the positions of the Se atoms (and hence residue 246) within the cluster. Although the presence of Cu(I) bound in the CXXC motif of domain 1 degrades the information available at the copper edge of the WT 245-Sec protein since it represents the average of D1 and D3 interactions, the data allow a number of new features of the cluster to be clearly identified. The Se−Cu interaction extracted from the Se edge data shows two Se−Cu interactions at 2.40 Å. Fits using lower Se−Cu coordination numbers produce higher least-squares residuals and, more importantly, lead to unacceptable fits to the Cu-edge data. This model predicts that each Se sees two Cu atoms in its first shell and therefore must occupy a bridging position in the cluster. In previous papers, we have argued that the simple model of a bis-cysteinyl bridged diCu(I) cluster with two bridging and one terminal Cys per Cu(I) (Figure 10A) cannot be correct as the Cu−Cu DW factors were inconsistent with this model (*13, 14*). From these data, the simple dinuclear cluster with two bridging Se atoms would require each Cu to be coordinated to two Se atoms and one S. Attempts to fit the Cu-edge data to this model, using the Cu−Se distances and DW factors extracted from the Se-edge, were routinely unsuccessful, leading to inconsistent analyses at the Cu- and Se-edges, respectively. However, when higher cluster nuclearity was introduced such as the structures shown in panels B and C of Figure 10, the Cu- and Se-edge data could be simulated with parameters which were consistent at both edges. In particular, the Cu EXAFS of the C22AC25A CCS-245Sec protein, which contains only the multinuclear cluster, yielded two Cu−S, one Cu−Se, and three Cu−Cu interactions, exactly matching the average distribution of scatterers per Cu absorber predicted for the $Cu_4Se_2S_4$ cluster (Figure 10C).

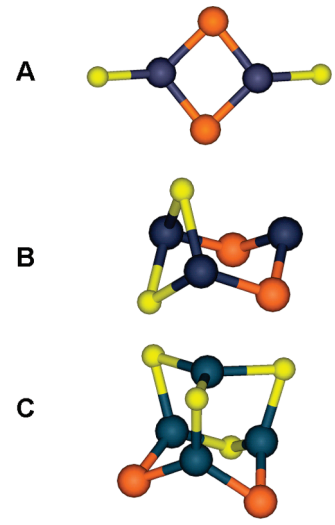

FIGURE 10: Simplified structural models for the hCCS cluster of increasing complexity and nuclearity.

Mindful of the fact that M−M interactions between heavy atom scatters can be difficult to distinguish, we also searched for fits to the data which included both Se−Cu and Se−Se components. An alternative minimum was discovered with two Se−Cu bonds at 2.36 Å and 0.7 Se−Se bond at 2.40 Å. Given the fact that the apoproteins exist partially in the diselenide form, it is possible that this solution represents a fraction of the sample which is still present as a diselenide even after TCEP reduction and is thus unable to coordinate Cu(I) at the D3−D3 interface. However, for this to be the case, only one-third of the total Se present in the sample would be available for coordination to Cu, and since this residual Se sees an average of two Se−Cu interactions, each Se in the Cu cluster would necessarily be coordinated by six Cu ions Although μ_4-selenido-bridged copper clusters have been identified (*51*), this seems to be an unlikely component of our cluster and is inconsistent with the Cu EXAFS data. Alternatively, the Se−Se component could be present within the copper cluster.

The chemistry of Cu(I)−selenolate systems is not extensive, but both terminal (*52*) and bridging (*53–55*) Cu(I)−selenolate interactions are well-documented. Bond lengths for both types are in the range of 2.30–2.45 Å and thus fully support the 2.38 ± 0.2 Å average Cu−Se interaction found in both solutions found for the Se EXAFS of the D1 mutant. In many cases, the simpler Cu_4S_X adamantane-type clusters which are common in Cu(I)−sulfur chemistry give way to multiatom cages of Se and Cu interlocking to form complex oligomeric and polymeric structures (*56, 57*). An interesting exception is a recent structure of a ferrocenyldiselenolate-stabilized Cu_2Se_2 cluster exhibiting a bis-selenolate bridged di-Cu(I) core in which each Cu(I) is three-coordinate with two bridging selenolates and one terminal phosphine ligand (*53*). The Cu−Se and Cu−Cu bond lengths are 2.40 and 2.62 Å, respectively, close to the metrical parameters observed for the CCS cluster. Notably absent, even in the supramolecular cage structures, are examples of complexes where Cu−Se and Se−Se bonds in the range of 2.3−2.45 Å coexist in a single cluster. On the basis of these comparisons, we

conclude that while it is not possible to accurately predict the structure of the Cu−Se-containing structure, it is unlikely that Se−Cu and Se−Se bonds are constituents of the same cluster, and we favor the interpretation in which each Se is bonded solely to two Cu(I) atoms.

In summary, we have successfully prepared Sec-substituted hCCS derivatives which accurately reproduce the activity and structural attributes of the native Cys-containing proteins. Merging of data from the Cu and Se EXAFS spectra is most consistent with the formation of a multinuclear Cu(I) cluster best formulated as $Cu_4Se_2S_4$. We believe this to be the first Se-containing Cu(I) cluster reported in a protein environment. This system is likely to have great utility in studying the mechanism of metal transfer between CCS and SOD as it provides an XAS probe of Cu binding to the CCS protein and can thus be used to monitor transfer of Cu out of the CCS-specific Se environment into its partner SOD. Further work is underway to fully exploit the mechanistic opportunities provided by this system.

ACKNOWLEDGMENT

We thank Andrew Bauman and Kristin Kutara for help in collection of XAS data, Martina Ralle for collection and interpretation of mass spectral data, and Mary Mayfield Gamble for help with the construction of mutant proteins. We gratefully acknowledge the use of facilities at the Stanford Synchrotron Radiation Laboratory which is supported by the National Institutes of Health Biomedical Research Technology Program, Division of Research Resources, and by the U.S. Department of Energy, Basic Energy Sciences (BES), and Office of Biological and Environmental Research.

SUPPORTING INFORMATION AVAILABLE

One table (Table S1) showing global EXAFS fitting results for the C22AC25A variant of CCS245Sec and one figure (Figure S1) showing the Cu K-absorption edges of CCS245Sec and its C22AC25A variant. This material is available free of charge via the Internet at http://pubs.acs.org.

REFERENCES

1. Culotta, V. C., Klomp, L. W. J., Strain, J., Casareno, R. L. B., Krems, B., and Gitlin, J. (1997) The copper chaperone for superoxide dismutase. *J. Biol. Chem. 272*, 23469–23472.
2. Culotta, V. C., Yang, M., and O'Halloran, T. V. 2006) Activation of superoxide dismutases: Putting the metal to the pedal. *Biochim. Biophys. Acta 1763*, 747–758.
3. Huffman, D. L., and O'Halloran, T. V. (2001) Function, structure, and mechanism of intracellular copper trafficking proteins. *Annu. Rev. Biochem. 70*, 677–701.
4. Rosenzweig, A. C. (2001) Copper delivery by metallochaperone proteins. *Acc. Chem. Res. 34*, 119–128.
5. Schmidt, P. J., Kunst, C., and Culotta, V. C. (2000) Copper activation of superoxide dismutase 1 (SOD1) in vivo. Role for protein-protein interactions with the copper chaperone for SOD1. *J. Biol. Chem. 275*, 33771–33776.
6. Schmidt, P. J., Rae, T. D., Pufahl, R. A., Hamma, T., Strain, J., O'Halloran, T. V., and Culotta, V. C. (1999) Multiple protein domains contribute to the action of the copper chaperone for superoxide dismutase. *J. Biol. Chem. 274*, 23719–23725.
7. Hall, L. T., Sanchez, R. L., Holloway, S. P., Zhu, H., Stine, J. E., Lyons, T. J., Demeler, B., Schirf, V., Hansen, J. C., Nersissian, A. M., Valentine, J. S., and Hart, P. J. (2000) X-ray crystallographic and ultracentrifugation analyses of truncated and full-length copper chaperones for SOD (LYS7). A dimer-dimer model of LYS7-SOD association and copper delivery. *Biochemistry 39*, 3611–3623.
8. Lamb, A. L., Torres, A. S., O'Halloran, T. V., and Rosenzweig, A. C. (2001) Heterodimeric structure of superoxide dismutase in complex with its metallochaperone. *Nat. Struct. Biol. 8*, 751–755.
9. Lamb, A. L., Wernimont, A. K., Pufahl, R. A., Culotta, V. C., O'Halloran, T. V., and Rosenzweig, A. C. (1999) Crystal structure of the copper chaperone for superoxide dismutase. *Nat. Struct. Biol. 6*, 724–729.
10. Lamb, A. L., Wernimont, A. K., Pufahl, R. A., O'Halloran, T. V., and Rosenzweig, A. C. (2000) Crystal structure of the second domain of the human copper chaperone for superoxide dismutase. *Biochemistry 39*, 1589–1595.
11. Caruano-Yzermans, A. L., Bartnikas, T. B., and Gitlin, J. D. (2006) Mechanisms of the copper-dependent turnover of the copper chaperone for superoxide dismutase. *J. Biol. Chem. 281*, 13581–13587.
12. Schmidt, P. J., Ramos-Gomez, M., and Culotta, V. C. (1999) A gain of superoxide dismutase (SOD) activity obtained with CCS, the copper metallochaperone for SOD1. *J. Biol. Chem. 274*, 36952–36956.
13. Stasser, J. P., Eisses, J. F., Barry, A. N., Kaplan, J. H., and Blackburn, N. J. (2005) Cysteine-to-serine mutants of the human copper chaperone for superoxide dismutase reveal a copper cluster at a domain III dimer interface. *Biochemistry 44*, 3143–3152.
14. Stasser, J., Siluvai, G. S., Barry, A. N., and Blackburn, N. J. (2007) A multinuclear copper (I) cluster forms the dimerization interface in copper-loaded human copper chaperone for superoxide dismutase. *Biochemistry 46*, 11845–11856.
15. Rae, T. D., Torres, A. S., Pufahl, R. A., and O'Halloran, T. V. (2001) Mechanism of Cu, Zn-superoxide dismutase activation by the human metallochaperone hCCS. *J. Biol. Chem. 276*, 5166–5176.
16. Furukawa, Y., Torres, A. S., and O'Halloran, T. V. (2004) Oxygen-induced maturation of SOD1: A key role for disulfide formation by the copper chaperone CCS. *EMBO J. 23*, 2872–2881.
17. Brown, N. M., Torres, A. S., Doan, P. E., and O'Halloran, T. V. (2004) Oxygen and the copper chaperone CCS regulate posttranslational activation of Cu,Zn superoxide dismutase. *Proc. Natl. Acad. Sci. U.S.A. 101*, 5518–5523.
18. Eisses, J. F., Stasser, J. P., Ralle, M., Kaplan, J., and Blackburn, N. J. (2000) Domains I and III of the human copper chaperone for superoxide dismutase interact via a cysteine-bridged dicopper cluster. *Biochemistry 39*, 7337–7342.
19. Peariso, K., Zhou, Z. S., Smith, A. E., Matthews, R. G., and Penner-Hahn, J. E. (2001) Characterization of the zinc sites in cobalamin-independent and cobalamin-dependent methionine synthase using zinc and selenium X-ray absorption spectroscopy. *Biochemistry 40*, 987–993.
20. Conradson, S. D., Burgess, B. K., Newton, W. E., Di Cicco, A., Filipponi, A., Wu, Z. Y., Natoli, C. R., Hedman, B., and Hodgson, K. O. (1994) Selenol binds to iron in nitrogenase iron-molybdenum cofactor: An extended X-ray absorption fine structure study. *Proc. Natl. Acad. Sci. U.S.A. 91*, 1290–1293.
21. Ralle, M., Berry, S. M., Nilges, M. J., Gieselman, M. D., van der Donk, W. A., Lu, Y., and Blackburn, N. J. (2004) The selenocysteine-substituted blue copper center: Spectroscopic investigations of Cys112SeCys *Pseudomonas aeruginosa* azurin. *J. Am. Chem. Soc. 126*, 7244–7256.
22. McCord, J. M., and Fridovich, I. (1969) Superoxide dismutase. An enzyme function for erythrocuprein (hemocuprein). *J. Biol. Chem. 244*, 6049–6055.
23. George, G. N. (1990) *EXAFSPAK*,Stanford Synchrotron Radiation Laboratory, Menlo Park, CA.
24. Binsted, N., Gurman, S. J., and Campbell, J. W. (1998) *EXCURVE*, version 9.2, Daresbury Laboratory, Warrington, England.
25. Gurman, S. J., Binsted, N., and Ross, I. (1984) A rapid, exact, curved-wave theory for EXAFS calculations. *J. Phys. C 17*, 143–151.
26. Gurman, S. J., Binsted, N., and Ross, I. (1986) A rapid, exact, curved-wave theory for EXAFS calculations. II. The multiple-scattering contributions. *J. Phys. C 19*, 1845–1861.
27. Binsted, N., and Hasnain, S. S. (1996) State of the art analysis of whole X-ray absorption spectra. *J. Synchrotron Radiat. 3*, 185–196.
28. Blackburn, N. J., Rhames, F. C., Ralle, M., and Jaron, S. (2000) Major changes in copper coordination accompany reduction of peptidylglycine monooxygenase. *J. Biol. Inorg. Chem. 5*, 341–353.
29. Ralle, M., Lutsenko, S., and Blackburn, N. J. (2003) X-ray absorption spectroscopy of the copper chaperone HAH1 reveals a

linear 2-coordinate Cu(I) center capable of adduct formation with exogenous thiols and phosphines. *J. Biol. Chem. 278*, 23163–23170.
30. Wilken, J., and Kent, S. B. H. (1998) Chemical protein synthesis. *Curr. Opin. Biotechnol. 9*, 412–426.
31. Kochendoerfer, G. G., and Kent, S. B. H. (1999) Chemical protein synthesis. *Curr. Opin. Chem. Biol. 3*, 665–671.
32. Cotton, G. J., and Muir, T. (1999) Peptide ligation and its application to protein engineering. *Chem. Biol. 6*, R247–R256.
33. Berry, S. M., Ralle, M., Low, D. W., Blackburn, N. J., and Lu, Y. (2003) Probing the role of axial methionine in the blue copper center of azurin with unnatural amino acids. *J. Am. Chem. Soc. 125*, 8760–8768.
34. Pickering, I. J., George, G. N., Fleet-Stalder, V., Chasteen, T. G., and Prince, R. G. (1999) X-ray absorption spectroscopy of selenium-containing amino acids. *J. Biol. Inorg. Chem. 4*, 791–794.
35. Low, S., and Berry, M. J. (1996) Knowing when not to stop: Selenocysteine incorporation in eukaryotes. *Trends Biochem. Sci. 21*, 203–208.
36. Gasdaska, J. R., Harney, J. W., Gadaska, P. Y., Powis, G., and Berry, M. J. (1999) Regulation of human thioredoxin reductase expresson and activity by 3′-untranslated region selenocysteine insertion sequence and mRNA instability elements. *J. Biol. Chem. 274*, 25379–25385.
37. Arner, E. S., Sarioglu, H., Lottspeich, F., Holmgren, A., and Bock, A. (1999) High-level expression in *Escherichia coli* of selenocysteine-containing rat thioredoxin reductase utilizing gene fusions with engineered bacterial-type SECIS elements and co-expression with the selA, selB and selC genes. *J. Mol. Biol. 292*, 1003–1016.
38. Johansson, L., Chen, C., Thorell, J. O., Fredriksson, A., Stone-Elander, S., Gafvelin, G., and Arner, E. S. (2004) Exploiting the 21st amino acid-purifying and labeling proteins by selenolate targeting. *Nat. Methods 1*, 61–66.
39. Hondal, R. J., Nilsson, B. L., and Raines, R. T. (2001) Selenocysteine in native chemical ligation and expressed protein ligation. *J. Am. Chem. Soc. 123*, 5140–5141.
40. Berry, S. M., Gieslelman, M. D., Nilges, M. J., van der Donk, W. A., and Lu, Y. (2002) An engineered azurin variant containing a selenocysteine copper ligand. *J. Am. Chem. Soc. 124*, 2084–2085.
41. Eckenroth, B., Harris, K., Turanov, A. A., Gladyshev, V. N., Raines, R. T., and Hondal, R. J. (2006) Synthesis and characterization of mammalian thioredoxin reductase. *Biochemistry 45*, 5158–5170.
42. Quaderer, R., Sewing, A., and Hilvert, D. (2001) Selenocysteine-mediated native chemical ligation. *Helv. Chim. Acta 84*, 1197–1206.
43. Gieselman, M. D., Xie, L., and van der Donk, W. A. (2001) Synthesis of a selenocysteine-containing peptide by native chemical ligation. *Org. Lett. 3*, 1331–1334.
44. Metanis, N., Keinan, E., and Dawson, P. E. (2006) Synthetic seleno-glutaredoxin 3 analogues are highly reducing oxidoreductases with enhanced catalytic efficiency. *J. Am. Chem. Soc. 128*, 16684–16691.
45. Stadtman, T. C. (1996) Selenocysteine. *Annu. Rev. Biochem. 65*, 83–100.
46. Zhong, L., Arner, E. S., and Holmgren, A. (2000) Structure and mechanism of mammalian thioredoxin reductase: The active site is a redox-active selenolthiol/selenenylsulfide formed from the conserved cysteine-selenocysteine sequence. *Proc. Natl. Acad. Sci. U.S.A. 97*, 5854–5859.
47. Gromer, S., Johansson, L., Bauer, H., Arscott, L. D., Rauch, S., Ballou, D. P., Williams, C. H., Jr., Schirmer, R. H., and Arner, E. S. (2003) Active sites of thioredoxin reductases: Why selenoproteins? *Proc. Natl. Acad. Sci. U.S.A. 100*, 12618–12623.
48. Aslund, F., Berndt, K. D., and Holmgren, A. (1997) Redox potentials of glutaredoxins and other thiol-disulfide oxidoreductases of the thioredoxin superfamily determined by direct protein-protein redox equilibria. *J. Biol. Chem. 272*, 30780–30786.
49. Besse, D., Siedler, F., Diercks, T., Kessler, H., and Moroder, L. (1997) The redox potential of selenocystine in unconstrained cyclic peptides. *Angew. Chem., Int. Ed. 36*, 883–885.
50. Ferguson, A. D., Labunskyy, V. M., Fomenko, D. E., Arac, D., Chelliah, Y., Amezcua, C. A., Rizo, J., Gladyshev, V. N., and Deisenhofer, J. (2006) NMR structures of the selenoproteins Sep15 and SelM reveal redox activity of a new thioredoxin-like family. *J. Biol. Chem. 281*, 3536–3543.
51. Yam, V. W.-W., Lo, K. K.-W., and Cheung, K.-K. (1996) A novel luminescent μ_4-selenido-bridged copper(I) tetramer. *Inorg. Chem. 35*, 3459–3462.
52. Lobana, T. S., Rimple, Castineiras, A., and Turner, P. 2003) Copper-selenium interactions: Influence of alkane spacer and halide anion in the synthesis of unusual polynuclear copper(I) complexes with bis(diphenylselenophosphinyl)alkanes. *Inorg. Chem. 42*, 4731–4737.
53. Nitschke, C., Fenske, D., and Corrigan, J. F. (2006) Ferrocenyldiselenolate-stabilized copper-selenium clusters. *Inorg. Chem. 45*, 9394–9401.
54. Christuk, C. C., Ansari, M. A., and Ibers, J. A. (1992) Interactions of coinage-group cations with the tetraselenotungstate anion: Multinuclear NMR spectroscopic results and crystal structures of $(\mu\text{-}WSe_4)[PMe_2Ph)_2Cu]_2$, $(\mu\text{-}WSe_4)[PMePh_2)Au]_2$ and $(\mu_3\text{-}Cl)(m_3\text{-}WSe_4)[(PPh_3)Cu]_3$. *Inorg. Chem. 31*, 4365–4369.
55. Salm, R. J., and Ibers, J. A. (1994) Synthesis, structure, and spectroscopy of $[PPh_4]_2[(NC)Cu(\mu\text{-}Se)_2M(\mu\text{-}Se)_2Cu(CN)]\cdot CH_3CN$ and $[PPh_4]_2[(NC)Cu(\mu\text{-}Se)_2MSe_2$ (M = Mo, W). *Inorg. Chem. 33*, 4216–4220.
56. Deveson, A., Dehnen, S., and Fenske, D. (1996) Synthesis and structures of four new copper(I)-selenium clusters: Size dependence of the cluster on the reaction conditions. *J. Chem. Soc., Dalton Trans. 1997*, 4491–4497.
57. Liu, C. W., Hung, C. M., Santra, B. K., Wang, J. C., Kao, H. M., and Lin, Z. (2003) Ligand substitution in cubic clusters: Surprising isolation of the cocrystallization products of $Cu_8(\mu_8\text{-}Se)[S_2P(OEt)_2]_6$ and $Cu_6[S_2P(OEt)_2]_6$. *Inorg. Chem. 42*, 8551–8556.

BI8001049